

# Statistical properties of charged interfaces

S. Teber

December 20, 2018

Laboratoire de Physique theorique et Modeles Statistiques, Batiment 100,  
Universite Paris-Sud, 91406, Orsay-Cedex, France

## Abstract

We consider the equilibrium statistical properties of interfaces submitted to competing interactions; a long-range repulsive Coulomb interaction inherent to the interface and a short-range, anisotropic, attractive one due to either elasticity or confinement. We focus on charged strings. Model systems considered for applications are mainly aggregates of solitons in polyacetylene and other charge density wave systems, domain lines in uniaxial ferroelectrics and the stripe phase of oxides. At zero temperature, we find a shape instability of the string due to the competing interactions. The instabilities lead, via phase transitions, to tilted phases as ground states of the string. Depending on the regime, elastic or confinement, the order of the zero-temperature transition changes. Thermal fluctuations lead in both cases to the roughening of the charged string and the presence of kinks in the angular sector. We suggest that such instabilities might explain the tilting of stripes in cuprate oxides. The 3D problem of the charged wall is also analyzed. The latter experiences instabilities towards a tilted phase in the elastic regime. In the confinement regime, the increase of dimensionality favors the melting of the wall into a Wigner crystal of its constituent charges. However, the solitonic lattice could be present in the form of a wall with a definite, non-zero, tilt angle as actually seen in nickelate oxides.

## 1 Introduction

Various types of systems in Nature display peculiar properties due to competing long-range forces. In this paper we focus mainly on the statistical properties of one-dimensional charged interfaces, in Ising-like systems, such as aggregates of charged topological defects in polyacetylene and other charge-density wave systems [1], charged domain-lines in uniaxial ferroelectrics [2] or stripes in oxides [3], [4]. Instabilities, such as the observed inclination of stripes in cuprates [5] and manganese [6], might be related to the presence of the long range Coulomb interactions and its competition with an attractive force. Uniaxial ferroelectrics and density waves are also model systems where such instabilities could take place.

The present study also deals with the more general case of two-dimensional charged interfaces, i.e. domain walls. They might be present, due to a dimensional crossover which induces a  $3D$  ordering, in the systems cited above. Also the latter case might find some applications in the field of biophysics for the study of membranes where electrostatic interactions play an important role, even though the interesting topological nature of the interface is lost.

The above interests emerged from a model-independent theory concerning the statistics and thermodynamics of uncharged and charged solitons which has been studied, respectively, in [7] and [8]. The system considered is two-fold degenerate and, when topologically doped, the solitons form a one-component plasma in either 2 or  $3D$  space. The competition between the long-range  $3D$  Coulomb interaction of the particles and the confinement force between them has led to a very rich phase diagram. Particularly interesting was the regime where the temperature is much less than the confinement energy scale, so that the solitons are actually bound into pairs, and the repulsive Coulomb interaction is weak enough to preserve these bisolitons as the elementary particles. In this regime, aggregated phases of bisolitons were shown to exist. The study of such aggregates in the continuum limit is equivalent to the study of charged interfaces. In the general case we consider such interfaces in the elastic regime. The elastic interaction is anisotropic which gives rise to an anisotropy axis along which the interface is aligned. A similar effect is given by a confinement force which appears beyond the elastic approximation. This confinement regime is relevant to quasi-one dimensional systems in relation with the statistics of solitons mentioned above. In both regimes the Coulomb interaction favors the inclination of the interface with respect to the anisotropy axis. This leads to zero-temperature instabilities with respect to a tilting of the interface. New ground-states of the system thus emerge from the competing interactions. The direct application to stripes in cuprates relies on the experimental observation that upon doping the system, at low temperatures, a transition from a collinear, i.e. vertical, to a diagonal stripe phase takes place [5]. The similarity with our actual results is thus striking.

The paper is organized as follows. We will mainly concentrate on the statistics of a charged string. In section 2 we present the models of the confined and elastic charged strings. In section 3 we derive the statistics of the string with the help of a saddle-point calculation. We present the zero-temperature results dealing with the instabilities of the string. In section 4 the effect of thermal fluctuations is considered. In section 5 the previous results are confirmed with the help of a numerical approach. In section 6 the present study is applied a model system [2]. Finally, in section 7 we consider the analogous  $3D$  problem concerning a charged plane.

## 2 Elastic and confinement regimes for the charged string

The problem of the charged string [8] has emerged from the study of the statistics of topological defects, i.e. solitons, common to charge density wave (CDW) systems. These general arguments are reproduced in the following as they give a full meaning to the physical origins of the present theory, cf. [10] for a review on the physics of topological defects in CDW systems. It should however be clear that this study is also relevant to other systems with discrete symmetry breaking as has been mentioned already in the Introduction.

For the moment we consider a one-dimensional system, i.e. a single chain, in a CDW state. The latter is described by a lattice order parameter which is complex in general

$$\Delta(x) = |\Delta(x)| \exp(i\varphi(x))$$

where  $x$  runs along the chain,  $|\Delta(x)|$  is related to the CDW gap and  $\varphi(x)$  fixes the position of the CDW with respect to a host lattice. In weakly commensurate CDW the low energy excitations are excitations of the phase. This leads, cf. [9], to a sine-Gordon type Hamiltonian

$$H = \int dx \left( \frac{\hbar v_F}{2\pi} \left( \frac{\partial \varphi}{\partial x} \right)^2 - W \cos(M\varphi) \right) \quad (1)$$

where the first term gives the elastic energy of the CDW and the second term reflects the pinning of the CDW superstructure by the host lattice;  $M$  is the degeneracy of the ground-state.

The non-trivial solutions of the equation of motion associated with (1) are the solitons, i.e. the  $\varphi$ -particles [11], which may be viewed as compressions or dilatations of the CDW. As we are in the realm of electronic crystals the solitons might therefore carry a charge which is fractional, i.e.  $q = 2/M$ , in the general case. For a double-degenerate ground state,  $M = 2$ , they are given by

$$\varphi(x) = 2 \arctan(\exp(2x/\xi)) \quad (2)$$

where the length  $\xi \sim \sqrt{\hbar v_F/W}$  corresponds to the width of this nucleus domain wall connecting the two ground states  $\varphi(\pm\infty) = \pm 1$ .

The situation is slightly different for the two-fold degenerate trans-polyacetylene because in this case the band is half-filled and the system is commensurate. In particular (1) does not describe this case. However the previous arguments remain qualitatively the same. The defect is an amplitude or  $\pi$ -soliton; it carries an integer charge and is described by

$$\Delta(x) = \Delta_0 \tanh(x/\xi) \quad (3)$$

where  $\Delta_0$  is a constant deformation of the chains. Again this excitation connects the two ground states of the system  $\Delta(\pm\infty) = \pm\Delta_0$ .

For a quasi-one-dimensional system, which we consider here, neighboring chains must have the same phase modulo  $2\pi$ . This leads to the following general two-particle interaction

$$E(\delta x) = -V \int dz \Delta_\alpha(\delta x - z) \Delta_\beta(z) \quad (4)$$

between neighboring chains  $\alpha$  and  $\beta$ , with coupling constant  $V$ , and solitons distant by  $\delta x$ . In the coarse-grained regime,  $\delta x \gg \xi$ , (4) grows linearly,  $E \approx V\delta x$ , a signature of the confinement of the defects. This can be shown explicitly with the help of (3) and (4). Dealing with a string, e.g. a domain line of solitons, this confinement energy is equivalently reproduced by the Solid on Solid (SOS) model. The related Hamiltonian reads

$$H_{conf} = \frac{J_\perp}{a_y} \sum_{y=0}^{L-1} |x_{y+1} - x_y| \quad (5)$$

where we have taken  $J_\perp = Va_y$  as the inter-chain energy scale,  $y$  runs along the vertical direction and  $x_y$  is an integer variable giving the deviation of the string with respect to the  $y$  axis.

The opposite case, corresponding to small deviations  $\delta x \ll \xi$ , is more general for the energy then increases quadratically  $E \approx V\delta x^2$ . This is equivalent to the elastic model which is extensively used in interface physics. The related Hamiltonian reads

$$H_{elast} = J_\perp \int \frac{dy}{a_y} \left( \frac{dx}{dy} \right)^2. \quad (6)$$

These two interface models are well known [12]. To compactify notations we shall define

$$H_{0p} = J_\perp \int \frac{dy}{a_y^p} \left| \frac{dx}{dy} \right|^p \quad (7)$$

where  $p = 1, 2$  leading respectively to the confinement and elastic regimes and where the continuum limit has been taken in both cases. We thus see that a crossover (corresponding to fractional  $1 < p < 2$ ) from the elastic to the confinement regime takes place as the distance between solitons increases, i.e. as the tilt angle of the string increases. This is manifested by the fact that  $\delta x = (dx/dy)a_y = \zeta a_y$  where  $\zeta$  is related to the tilt angle of the string and  $a_y$  is the inter-chain distance. For  $\zeta \ll \xi/a_y$  the string is elastic whereas for  $\zeta \gg \xi/a_y$  the confined string is relevant. The crossover between the two regimes takes place at

$$\zeta_0 = \xi/a_y. \quad (8)$$

The introduction of the 3D long-range Coulomb interaction yields

$$H_c = \frac{(ze)^2}{2\epsilon} \int \int dy dy' \left( \frac{1}{\sqrt{(y-y')^2 + (x(y) - x(y'))^2}} - \frac{1}{\sqrt{(y-y')^2}} \right) \quad (9)$$

where  $z \leq 1$  so that the elementary constituent of the string might carry a fractional charge  $ze$  ( $z = 1$  for polyacetylene),  $\epsilon$  is the dielectric constant of the isotropic, neutral media in which the plane is embedded and the contribution of the vertical string has been subtracted.

The thermodynamics of the charged interface is governed by  $H_p = H_{0p} + H_c$  or explicitly

$$H_p = J_\perp \int \frac{dy}{a_y^p} \left| \frac{dx}{dy} \right|^p + \frac{(ze)^2}{2\epsilon} \int \int dy dy' \left( \frac{1}{\sqrt{(y-y')^2 + (x(y)-x(y'))^2}} - \frac{1}{|y-y'|} \right). \quad (10)$$

### 3 The charged string at zero temperature

#### 3.1 The saddle point approximation

We consider a configuration

$$x(y) = x^{(0)}(y) + \delta x(y) \quad (11)$$

were  $x(y)$  has been expanded in the vicinity of the saddle point distribution  $x^{(0)}(y)$  with deviations  $\delta x(y)$ . Free boundary conditions are taken. The expanded Hamiltonian reads, in the harmonic approximation

$$H_p = H_p^{(0)} + \frac{1}{2} \int \int dy dy' \delta x(y) \delta^{(2)} H / \delta x(y) \delta x(y')|_{\delta x=0} \delta x(y') + \dots \quad (12)$$

where  $H_p$  is given by (10) and  $H_p^{(0)} \equiv H_p\{\delta x^{(0)}(y)\}$ . The saddle point distribution is given by  $\delta H_p / \delta x(y) = 0$  that is

$$J_\perp p \left( \Delta x^{(0)}(y) \right)^{p-1} = \frac{(ze)^2}{2\epsilon} \int_{-\infty}^{+\infty} dy' \frac{x^{(0)}(y') - x^{(0)}(y)}{\left( (y-y')^2 + (x^{(0)}(y) - x^{(0)}(y'))^2 \right)^{3/2}}. \quad (13)$$

This non-linear integro-differential equation cannot be solved exactly. We will therefore take an ansatz for the ground-state configuration  $x^{(0)}(y)$  of the string. As can be seen from (10), at zero temperature, the elastic or confinement term favors a vertical string, i.e. along the  $y$  axis, whereas the Coulomb favors the disintegration of the string in the perpendicular direction. Instabilities of the string arise from the competition between these interactions. *We find that these instabilities lead to a tilted string as the new ground state of the system.* Therefore

$$x^{(0)}(y) = \zeta y \quad (14)$$

were  $\zeta = \tan \theta$ ,  $\theta$  being the tilt angle of the string with respect to the  $y$  axis. This ansatz satisfies the linearized equation (13) up to some logarithmic corrections. As will be shown explicitly in the following,  $\zeta$  is related to the ratio between

the Coulomb and confinement or elastic energy scales. It is thus related to the elementary charge of the string constituent soliton.

With the help of (14), and (10), (12) reads

$$H_p = H_p^{(0)} + \sum_k \lambda_{p,k}^2(\zeta_p) |\delta x_k|^2 \quad (15)$$

with the eigenvalues

$$\lambda_{p,k}^2(\zeta_p) = k^2 J_\perp \left( p(p-1) + \frac{2\zeta_p^2 - 1}{[1 + \zeta_p^2]^{\frac{5}{2}}} \gamma(k) \right). \quad (16)$$

$\zeta_p$  is the optimal angle corresponding to the distribution (14) minimizing  $H_p^{(0)}$  and

$$\gamma(k) = \gamma_0 \log(1/ka) \quad (17)$$

with

$$\gamma_0 = \frac{(ze)^2}{2\epsilon a_y J_\perp} \quad (18)$$

being the ratio of the Coulomb to the elastic or confinement energy scales.

The first term in (15) corresponds to the mean-field Hamiltonian.  $H_p^{(0)}$  leads to the following mean-field free energy density

$$f_p^{(0)}(\zeta) = \frac{J_\perp}{a_y} \left[ \zeta^p + \gamma_D \left( \frac{1}{\sqrt{1 + \zeta^2}} - 1 \right) \right] \quad (19)$$

where  $\gamma_D = \gamma(l_D^{-1})$  and  $l_D$  is the Debye screening length taken into account as a hard cut-off to eliminate the logarithmic divergence of the Coulomb term in the thermodynamic limit. Details concerning the screening mechanisms and the expressions of  $l_D$  have been reported in Appendix A. As can be seen in the first term of (19) in the confinement regime, the absolute value has been dropped. This is the non-return approximation for the confinement regime the limitations of which will be considered at the end of this section. In the following subsections we will see how the tilted phase arises via zero-temperature phase transitions in both  $p = 1, 2$  regimes.

### 3.2 The elastic charged string

We first consider the elastic regime, with  $p = 2$  in (19), corresponding to tilt angles below the crossover value (8). Figure 1 displays this free energy as a function of the angle. Until

$$\gamma_D^c = 2 \quad (20)$$

the vertical line,  $\zeta_2 = 0$ , is stable. Above  $\gamma_D^c$  the vertical line becomes unstable and the free energy has a double well shape. This is due to the double degeneracy

Figure 1: 1) Mean-field free energy of the elastic string (19) as a function of  $\zeta$  exhibiting a second order phase transition. The two curves correspond to  $\gamma_D < \gamma_D^c$  where the vertical string is stable and  $\gamma_D > \gamma_D^c$  where the tilted line is stable as can be seen from the double well.

2) Free energy of the confined string as a function of  $\zeta$  exhibiting a first order transition from the vertical string to the free string. From upper to lower curve: free model  $\gamma_D = 0$ , metastable states appear when  $\gamma_D > \gamma_D^*$ , they become stable states when  $\gamma_D > \gamma_D^c$ .

of the system; the new, tilted, ground states corresponding to  $\pm\zeta_2$  have the same energies. The optimal angle reads

$$\zeta_2 = \sqrt{\left(\frac{\gamma_D}{2}\right)^{\frac{2}{3}} - 1}. \quad (21)$$

The transition at  $\gamma_D^c$  is second order. This can be shown by evaluating a quantity analogous to the heat capacitance in usual thermodynamic phase transitions. That is

$$C_\gamma = -\gamma_D \frac{\partial^2 f_2^{(0)}}{\partial \gamma_D^2} \quad (22)$$

with the tilt angle given by (21) above the transition and vanishing below. (22) yields

$$C_\gamma = \frac{2J_\perp}{9} \left(\frac{2}{\gamma_D}\right)^{2/3} \left[1 + \frac{1}{2} \left(\frac{\gamma_D}{2}\right)^{1/3}\right] \quad \gamma_D > \gamma_D^c$$

$$C_\gamma = 0 \quad \gamma_D < \gamma_D^c$$

which exhibits a jump at the transition,  $\Delta C_{\gamma_D^c} = J_\perp/3$ .

The linear stability analysis of these mean-field solutions can be performed by looking at (16) with  $p = 2$

$$\lambda_{2,k}^2(\zeta_2) = J_\perp k^2 \left(2 + \frac{2\zeta_2^2 - 1}{[1 + \zeta_2^2]^{\frac{5}{2}}} \gamma(k)\right). \quad (23)$$

These eigenvalues must be positive, for all momentum  $k$ , in order to ensure the stability of the solution.

Expanding first around the vertical line,  $\zeta_2 = 0$ , (23) leads to the following stability criterion

$$\gamma(k) = \gamma_0 \log(1/ka) < 2, \quad \forall k$$

or

$$k > k_c = \frac{1}{a} \exp(-2/\gamma_0)$$

where  $k_c$  is the Coulomb-dependent critical momentum. This shows that the instability is driven by low-momentum, i.e. long wavelength, modes. Reminding

that  $1/l_D < k < 1/a$ , we find, in agreement with the mean-field analysis, that the vertical string is stable as long as  $k_c < 1/l_D$ .  $k_c = 1/l_D$  returns us to (20). Increasing the strength of the Coulomb interaction increases  $k_c$ . For  $k_c > 1/l_D$  a continuous set of modes, i.e. between  $1/l_D$  and  $k_c$ , has negative eigenvalues so that the vertical string is no more stable.

Expanding around  $\xi_2 \neq 0$ , we see from (23), that all modes are stable as soon as  $\xi_2 > 1/\sqrt{2}$ . For such tilt angles we are of course above the critical point as can be seen with the help of (21). The tilted line is thus stable against harmonic fluctuations.

### 3.3 The confined charged string

When  $\zeta$  becomes larger than the crossover value  $\zeta_0$ , cf. (8), the elastic approximation is no more valid and we reach the peculiar confinement regime with  $p = 1$ . In this case the eigenvalues (16) are given by

$$\lambda_{1,k}^2(\zeta_1) = J_\perp \frac{2\zeta_1^2 - 1}{[1 + \zeta_1^2]^{\frac{5}{2}}} k^2 \gamma(k). \quad (24)$$

We see from (24) that configurations with  $\zeta_1 > 1/\sqrt{2} = \zeta_1^*$  are always stable against harmonic fluctuations. Moreover this is a pure Coulomb stability. On the other hand configurations with  $\zeta_1 < 1/\sqrt{2} = \zeta_1^*$  are always unstable. This implies that the stability of the vertical string cannot be analyzed within the present model. This is related to the non-return approximation made in (15). Numerical simulations however show that the tilted string is, here also, the new ground state, cf. section 4. In relation with the crossover between elastic and confinement regime we can then interpret  $\zeta_1^*$  as a low boundary for the crossover angle  $\zeta_0$ , cf. (8). In the following we will thus consider solutions corresponding to  $\zeta_1 > \zeta_1^*$ , i.e.  $\gamma_D > \gamma_D^*$ .

Figure 1 shows a crucial difference between the confinement and elastic regimes concerning the mechanism by which tilted strings, i.e. a double well in the free energy, appear. Contrary to the previous case the second derivative of the energy remains positive a signature of the fact that the correlation length remains finite and that the transition is first order in the confinement regime. Metastable states thus appear. We are going to show first that they appear at  $\gamma_D^*$ , the upper spinodal strength. From (19) with  $p = 1$ , the vanishing of the first derivative of the free energy density leads to

$$1 = \gamma_D \frac{\zeta_1}{(1 + \zeta_1^2)^{3/2}}. \quad (25)$$

The spinodal line, above which (metastable) solutions appear can be defined with the help of the coupled equations (25) and its derivative. This leads to

$$\zeta_1^* = \frac{1}{\sqrt{2}} \quad \gamma_D^* = \frac{3\sqrt{3}}{2} \approx 2.6$$

Increasing the Coulomb interaction we reach the critical regime where the mean-field free energy of the tilted solution becomes equal to that of the  $\zeta = 0$  solution  $f_1(\zeta = 0) = f_1(\zeta_1)$ . This equation together with (25) define the critical point and lead to

$$\zeta_1^c = \sqrt{\frac{1}{2} + \frac{\sqrt{5}}{2}} \approx 1.3 \quad \gamma_D^c \approx 3.3$$

As in critical phenomena, for  $\gamma_D > \gamma_D^c$ , the system jumps to the non-zero tilt angle solution corresponding to the absolute minimum of the energy.

## 4 The charged string at finite temperature

The results of the previous section concern the  $T = 0$  case. We seek, in the present section, for the effect of temperature. In the following we consider the low temperature regime where the string needs to be quantized. From the expression of the full free energy, thermodynamic quantities can be evaluated. We give the expression of the heat capacitance. Then we consider the effect of thermal fluctuations. The thermally assisted tunneling, a characteristic feature of the present double well problem, is manifested by the presence of kinks in the angular sector. The  $N$ -kink problem is defined and the energies of the 1- and 2-kink string configurations are given. The tunneling is then related to the lost of long-range order in the system. These considerations are completed by analyzing the thermal roughening of the charged string.

### 4.1 Thermodynamic quantities

Apart from a logarithmic correction the spectrum (16) is that of phonons, a feature of the saddle point approximation. We thus have a harmonic oscillator problem which is easily quantized

$$E_{\{n_k\}} = E^{(0)} + \sum_k (n_k + \frac{1}{2}) \omega_{k,p}$$

where the units has been chosen such that  $\omega_{k,p}$  has the dimension of an energy. This yields

$$f_p = f_p^{(0)} + T \int_{\frac{1}{l_D}}^{\frac{1}{a}} \frac{dk}{2\pi} \log(1 - \exp(-\omega_{k,p}/T)) + \frac{1}{2} \int_{\frac{1}{l_D}}^{\frac{1}{a}} \frac{dk}{2\pi} \omega_{k,p} \quad (26)$$

where the second term is an entropic contribution and the last corresponds to the zero point energy. The general expression of the free energy density is then

$$\begin{aligned} f_p = f_p^{(0)} & - \frac{T^2}{12\sqrt{J_\perp [p(p-1) + \gamma(\zeta)]}} + \frac{1}{4\pi a^2} \left\{ \sqrt{J_\perp p(p-1)} \right. \\ & \left. + \left( \frac{a}{l_D} \right)^2 \sqrt{J_\perp [p(p-1) + \gamma(\zeta) \ln(l_D/a)]} \right\} \end{aligned} \quad (27)$$

Figure 2: Angular kinks shapes. a) Exact kink shape. b) Point like kink. c) Shape of the string with  $N$ –kink excitations. d) Numerical result

$$+ \frac{1}{2} \left( \frac{\pi J_{\perp} \gamma(\zeta)}{2} \right)^{\frac{1}{2}} \left[ \operatorname{Erf} \left( \sqrt{\frac{2[p(p-1) + \gamma(\zeta) \ln(l_D/a)]}{\gamma(\zeta)}} \right) - \operatorname{Erf} \left( \sqrt{\frac{2p(p-1)}{\gamma(\zeta)}} \right) \right] \exp \left( \frac{2p(p-1)}{\gamma(\zeta)} \right) \right\}$$

where

$$\gamma(\zeta) = \gamma_0 \frac{2\zeta^2 - 1}{(1 + \zeta^2)^{5/2}}$$

and  $\gamma_0$  is given by (18).

It is simple, from (27), to compute the heat capacitance, at constant length, of the system. We obtain

$$C_L^{(p)} = \frac{T}{6 \sqrt{J_{\perp} \left[ p(p-1) + \gamma_0 \frac{2\zeta^2 - 1}{(\zeta^2 + 1)^{5/2}} \right]}} \quad (28)$$

which is linear in  $T$  with an angle dependent coefficient. Such an expression can be usefully compared with experimental work on related physical systems.

## 4.2 Thermal fluctuations: kink solution

Thermal fluctuations destroy the tilted phase. This proceeds via tunneling of the string from one ground-state to the other. This process is due to the presence of instantons in the angular sector. We shall call them angular kinks.

Coarse graining the system we consider the kink as a point-like excitation as in Figure 2b. This amounts to neglect it's core on the scale of which elastic or confinement energy compete with the Coulomb energy to connect smoothly the two ground states as shown in Figure 2a. At finite temperatures a general configuration of the string is thus similar to Figure 2c where an array of angular kinks is present. This shape agrees with the numerical results displayed on Figure 2d.

The energy of an array of  $N$  kinks is given by

$$\Delta E_N = \frac{J_{\perp} \gamma_0}{a_y} \sum_{i,j=0}^N \int_{t_i}^{t_{i+1}} dt \int_{t'_j}^{t'_{j+1}} dt' \frac{1}{\sqrt{(t-t')^2 + (x_{i+1}(t) - x_{j+1}(t'))^2}} - E_N^{(0)} \quad (29)$$

where  $t_{N+1} = -t_0 = +\infty$ , the other  $t_i$ 's denoting the position of the defects,  $x_i(t)$  is a portion of string connecting point  $t_{i-1}$  to point  $t_i$  and  $E_N^{(0)}$  is the Coulomb energy of the same string without kinks, i.e. at  $T = 0$ . The point-like kink approximation amounts to use the tilted ansatz ground state  $x_i(t) = (-1)^i \zeta(t - t_i) + x_i(t_i)$ . As it should be (29) vanishes for a zero tilt angle.

It also shows that the defect is a pure Coulomb kink. (29) is therefore available for both elastic and confinement models. This is consistent with the fact that these models have similar long distance properties as shown in Appendix B with the help of a transfer matrix approach. However, even though exact results can be obtained with the help of (29) within the limits of the point-like kink approximation, the obtained expressions, in the general case, are quite intractable. We will therefore consider simple cases.

First the 1–kink energy. The latter reads

$$\Delta E_1 = \frac{2J_\perp \gamma_0 L}{a_y \sqrt{1 + \zeta^2}} \ln \left[ \frac{1 + \sqrt{1 + \zeta^2}}{2} \right] \quad (30)$$

where  $2L$  is the length of the string. (30) shows that the angular-kink has an infinite energy. The thermodynamic limit is however well defined due to screening in the system, cf. Appendix A. As anticipated in the previous section this gives rise to an upper distance cut-off, the Debye length. We take it as a hard cut-off which regularizes (30) in the thermodynamic limit, i.e.  $L \rightarrow l_D$ . This gives a finite activation energy for the kink formation

$$\Delta E_1 = \frac{J_\perp \gamma_0 l_D}{a_y \sqrt{1 + \zeta^2}} \ln \left[ \frac{1 + \sqrt{1 + \zeta^2}}{2} \right].$$

Thus we have an exponentially small density of kinks

$$n \approx \exp \left( -\frac{\Delta E_1}{T} \right). \quad (31)$$

When  $T < \Delta E_1$  there is long range orientational order for the inclined string. When  $T \geq \Delta E_2$  kinks proliferate and the long range order is broken.

Next, we treat the 2–kink problem. When their separation is smaller than the screening length (29) yields

$$\begin{aligned} \Delta E_2 = & \frac{J_\perp \gamma_0}{a_y \sqrt{1 + \zeta^2}} \sum_{\epsilon=\pm} \epsilon \left\{ \delta t \log \left( \frac{\sqrt{(1 + \zeta^2)[(L + \delta t)^2 + \zeta^2(L - \epsilon \delta t)^2]} + L + \delta t + \zeta^2(L - \epsilon \delta t)}{2\delta t [1 + \zeta^2 \frac{1-\epsilon}{2}]} \right) \right. \\ & + \delta t \log \left( \frac{\sqrt{(1 + \zeta^2)[L^2 + \zeta^2(L - \delta t - \epsilon \delta t)^2]} + L + \zeta^2(L - \delta t - \epsilon \delta t)}{2\delta t [1 + \zeta^2 \frac{1-\epsilon}{2}]} \right) \quad (32) \\ & + L \log \left( \frac{\sqrt{(1 + \zeta^2)[(L + \delta t)^2 + \zeta^2(L - \epsilon \delta t)^2]} + L + \delta t + \zeta^2(\delta t - \epsilon L)}{2L [1 + \zeta^2 \frac{1-\epsilon}{2}]} \right) \\ & \left. + (L - \delta t) \log \left( \frac{\sqrt{(1 + \zeta^2)[L^2 + \zeta^2(L - \delta t - \epsilon \delta t)^2]} + L + \zeta^2(\delta t - \epsilon(L - \delta t))}{2(L - \delta t) [1 + \zeta^2 \frac{1-\epsilon}{2}]} \right) \right\}. \end{aligned}$$

The term with  $\epsilon = +1$  corresponds to the contribution of the kinky string whereas the one with  $\epsilon = -1$  is the subtraction of the ground-state string. When  $\delta t < l_D \ll L$ , (32) yields

$$\Delta E_2 \approx \frac{2J_\perp \gamma_0 \delta t}{a_y \sqrt{1 + \zeta^2}} \log(1 + \zeta^2) + \mathcal{O}\left(\left(\frac{\delta t}{L}\right)^2\right). \quad (33)$$

In the limit  $L \rightarrow \infty$  the angular bikink is stable. At the optimal angle (33) shows that this pair is confined with an energy growing linearly as a function of the transversal distance between the kinks.

Due to their non-trivial topological nature isolated kinks destroy the long-range orientational order. The effect of the 2-kink excitations is different. The latter are not activated. They appear as soon as  $T > 0$ . Their effect is to break the long-range positional order as they do not affect the orientation of the string. The proliferation of angular bikinks is therefore a signature of the thermal roughening of the charged string.

### 4.3 Thermal fluctuations: roughening

Given the density of kinks (31), the length of the string between two angular kinks is given by

$$l \approx \frac{1}{n}.$$

Within this length thermal fluctuations also play an important role. This has been anticipated in the previous subsection with the help of the bikinks. We consider here the difference correlation function which reads, with the help of (15), in the limit of large  $y$

$$\langle (\delta x(y) - \delta x(0))^2 \rangle_p \approx y \frac{T a_y}{J_\perp} \frac{1}{p(p-1) + \gamma(\zeta) \ln(y/a)} \left\{ 1 + \frac{\gamma(\zeta)}{p(p-1) + \gamma(\zeta) \ln(y/a)} + \dots \right\} \quad (34)$$

where the omitted terms are higher powers of the second term in brackets. Equation (34) shows that the charged string, which might be tilted if the Coulomb interaction is sufficiently strong, roughens at all non-zero temperatures. Hence, there is no positional order

$$\langle \delta x \rangle \sim \sqrt{\langle (\delta x(y) - \delta x(0))^2 \rangle_p} \approx \sqrt{y} \rightarrow \infty \quad y \rightarrow \infty$$

but there is long-range orientational order

$$\langle \delta \zeta \rangle \sim \frac{d \langle \delta x \rangle}{dy} \approx 1/\sqrt{y} \rightarrow 0 \quad y \rightarrow \infty.$$

This is analogous to the non-interacting case and is a characteristic feature of one dimensional interfaces. The string must be embedded in an external potential to give rise to a non-zero roughening temperature.

The results of this section and the previous will be clearly displayed within the numerical approach.

#### 4.4 Application to stripes in oxides

Following Wakimoto & al [5], we are going to recall briefly here some experimental results which might give relevance to the present theory. These results concern stripes observed, with the help of neutron-scattering measurements, in  $La_{2-x}Sr_xCuO_4$  oxides where  $x$  is the concentration of  $Sr$  dopants. The present work does not allow us to understand the microscopic phenomenons taking place in these systems, e.g. superconductivity and it's interplay with magnetism. We concentrate only on the long distance properties of this system, namely, the fact that stripes consist of lines of holes coming from the  $Sr$  dopants. The latter are thus charged strings as the ones described in this paper.

The experimental results are summarized on Figure 3 which has been taken from the work of Fujita & al [5]. In Figure 3 (a)  $\delta$  is of the order of the inverse distance between stripes. At low doping, the inset on the left of this figure, shows magnetic Bragg peaks corresponding to a one-dimensional spin modulation which is inclined with respect to the reference tetragonal axis. At higher doping, the inset on the left, shows that this spin modulation, along with the charge stripes, have rotated by an angle of 45 degrees. The main figure, together with Figure 3 (b) which displays the tilt angle as a function of the concentration of dopant, show that this shape instability takes place around  $x_c \approx 0.05$  where  $\delta$  increases linearly with  $x$ . Moreover, the authors report a weak dependence of the magnetic peaks on the third direction. This implies that the spin modulations are weakly correlated between successive  $CuO_2$  layers. Thus, the stripes can be considered with a good accuracy as charged strings. The case of 3D ordering where stripes form domain walls will be considered in section 7. The stripe instability observed experimentally might be due to the competition between the long-range Coulomb interaction and an anisotropic interaction. To relate this instability to an increase of the concentration of dopants  $x$  we should probably take into account structural changes. As argued by Tranquada & al [3], the lines of charge might be pinned along the direction of the tilt of the  $CuO_6$  octahedron. This tilt direction varies with doping. It is along the orthorhombic axis at low doping and along the tetragonal axis at higher doping. These axis are 45 degrees from each-other. At an intermediate doping, corresponding to the critical value  $x_c$ , a 45 degrees tilt of the stripes, satisfying the structural constraints, can take place.

Simple considerations related to the competing energy scales are in favor of such an order of magnitude for the tilt angle. First, in this system  $e^2/ea \sim 0.1 - 1eV$  where  $a$  is a unit length of the tetragonal structure. Second the exchange energy  $J_\perp$  is of the order of  $0.13eV$ . Thus  $\gamma_0 \sim 0.4 - 4.5$  where (18) has been used. If we consider that the Debye length is of the order of the inter-stripe distance  $1/\delta$ , at the transition  $x_c$  we have  $l_D \sim 20a$ . Thus  $\gamma_D = \gamma_0 \ln(l_D/a) \sim 1.2 - 13.5$ . Using (21), the maximum tilt angle compatible with these values is around 55 degrees. A tilt angle of 45 degrees can be reached with a  $\gamma_D \sim 4.0$  which is clearly in the range of allowed values above. Hence, the competing interactions can be responsible for such a tilt.

This tilt could reduce the electrostatic energy of the stripe as can be seen by the

Figure 3: Tilting of stripes in a cuprate oxide.

following argument. At low doping, i.e. in the diagonal stripe phase, the hole concentration along the stripe is 0.7 hole/Cu. This concentration is reduced to 0.5 hole/Cu in the collinear stripe phase, cf. Wakimoto & al. The density of charges along the stripe is thus reduced by  $\sqrt{1 + \zeta^2}$ , with  $\zeta = 1$  for the present 45 degrees tilt angle. This dilatation factor reduces the electrostatic energy of the string as has already been seen in (19). This could hold assuming that the number of holes/stripe is constant. The added dopants would lead to the formation of new stripes. The latter become tightly packed at high doping as suggested by the linear relation  $\delta \approx x$ .

## 5 Numerical approach

The statistics of the charged string in both elastic and confinement regimes has been studied with the help of a Montecarlo-Metropolis algorithm. These numerical simulations allow the computation of the properties of the full Hamiltonian (10) with open boundary conditions as above. The ground state is found with the help of a simulated annealing. The shape of the distribution, the value of the zero temperature order parameter  $\zeta$  and the energy of the distribution as a function of  $\gamma_0$  have been computed to detect the various instabilities and associated phase transitions. The effect of thermal fluctuations, i.e. the roughening and tunneling, have also been studied. These numerical results show good agreement with the analytical results presented above.

### 5.1 Elastic string

We focus first on the zero-temperature properties of the string. The ground-state has been found by performing a logarithmic simulated annealing during each Monte-Carlo simulation

$$T[i] = T[0] \frac{\ln 2}{\ln(2 + i)}$$

where  $i$  is the Monte-Carlo step and  $T[0]$  is a high initial temperature. Due to an improved algorithm to treat the Coulomb interaction the logarithmic decay of temperature has been successfully implemented in the simulations. As is well known this leads to the ground-state with the lowest probability of being trapped in metastable states.

We compute the properties of the full Hamiltonian (10). The numerical coupling constant in (9) is defined by  $\gamma_{num}$ . The rigidity  $J_\perp$  in (6) is taken to be unity. With these numerical coupling constants a comparison can be made with the analytical results obtained using a mean-field theory. In this respect  $\gamma_{num}$  should correspond to  $\gamma_0$  in (17). The computational cell needs of course to be finite and there is therefore no reason for using an upper cut-off limit  $l_D$ . Therefore

Figure 4: Absolute value of  $\zeta$  as a function of  $\gamma_{num}$

Figure 5: Shape of the string: below the transition the charged string is vertical. Above the transition it tilts away from the anisotropy axis.

$l_D \rightarrow L$  and  $\gamma_{num} = \gamma_D / \ln L$  which reflects the non-extensivity arising from the long-range interaction. In particular the critical numerical coupling constant should be given by  $\gamma_{num}^c = \gamma_D^c / \ln L = 2 / \ln L$  where (20) has been used.

We consider first the behavior of the order parameter  $\zeta$  as a function of  $\gamma_{num}$  for different sizes  $L$ . A typical result is displayed on figure 4. Each point in this figure corresponds to an independent Monte-Carlo simulation, i.e. given by generating a new random configuration which is then thermalized by the simulated annealing and brought to an effective zero temperature. Due to the double degeneracy of the ground state it is the absolute value of  $\zeta$  which has been plotted. The behavior is the one expected by the analytical results. Furthermore the critical coupling constant is given by  $\gamma_{num}^c$  with an error of the order of 1% as is given by fitting the numerical data with (21). Below the transition the mean angle is zero. A typical shape of the string in this region is given in Figure 5. The string is vertical in average. Above the transition the mean angle increases with  $\gamma_{num}$  in accordance with (21). The string is then tilted with respect to the main axis as shown also in Figure 5. No jump in the order parameter takes place which is an indication that the phase transition is second order. The energy of the string has however been computed as a function of  $\gamma_{num}$ . It is continuous. The second derivative is found on the other hand to diverge around the critical value.

Next we take into account thermal fluctuations. When the temperature is less than the activation energy of single angular kinks  $\Delta E_1$ , cf. (30), the line is rough as shown by Figure 6. Above  $\Delta E_1$  single angular kinks are present in addition to the roughening, cf. Figure 2. The orientational order is then lost. These results clearly confirm what has been said in the previous sections. At temperatures higher than  $\Delta E_1$ , thermal fluctuations average the tilt angle to zero.

## 5.2 Confined string

The same approach is performed with the confined string.

Figure 7 displays the absolute value of  $\zeta$  as a function of  $\gamma_{num}$ . The behavior is the same as in the previous case. The straight string is stable below the transition and tilts above. However a jump in the order parameter is noticeable (especially in comparison with the equivalent Figure 4 concerning the elastic

Figure 6: Rough inclined string at low temperature; orientational order is preserved.

Figure 7: Absolute value of  $\zeta$  as a function of  $\gamma_{num}$  in the confinement regime.

Figure 8: Energy of the string as a function of  $\gamma_{num}$ . The solid line corresponds to the energy of a string. A discontinuity is clearly noticeable. The diamonds correspond to the first derivative of the latter.

regime), an indication that the transition is first order. This is further confirmed by looking at the energy displayed on Figure 8. It is clearly discontinuous as a function of  $\gamma_{num}$  at the transition. The numerical study allows to capture the properties of the charged confined string in the whole range of  $\gamma_{num}$ . This is to be contrasted with the analytical work where we could not consider the small tilt angle region. In contrast with what has been said in [8] this regime is not manifested by an instability of the string towards a modulation. The ground state given by the numerical simulations is also the straight, either inclined or not, string.

At finite temperature the results for the confined regime are qualitatively the same as for the elastic one.

## 6 Link with the statistics of solitons

The present study should be connected, as has been said in the Introduction, to the previous work on the statistics of solitons. In quasi-one dimensional systems the string is composed of solitons which were able to aggregate due to the confinement. The results for the confinement regime, i.e.  $p = 1$ , are thus relevant here. We will first seek the stability of the string phase with respect to the Wigner crystal of solitons at  $T = 0$ . Then we will concentrate on the non-zero temperature regime and look for the shape of the aggregates of solitons which lead to strings.

### 6.1 Strings versus Wigner crystal of solitons

We consider first the case when  $T = 0$ . As the Coulomb interaction increases, the string of solitons tilts. Its energy also increases. This might lead to a dissociation of the string as soon as its energy per soliton  $\mu = \delta H^{(0)} / \delta N$  becomes larger than the energy of the constituent soliton  $\mu_{sol}$ . The latter corresponds to  $2J_{\perp}R/a_x + (ze)^2/\epsilon R$  where  $R \approx \sqrt{s/\nu}$  is the radius of the Wigner Seitz cell including the soliton and a background charge of density  $\nu/s$  with  $s = a_x a_y$ . This energy can also be written as

$$\mu_{sol} = \frac{2J_{\perp}R}{a_x} [1 + \nu\gamma_0]$$

where  $\gamma_0$  is given by (18). The ensemble of solitons is diluted, cf [7], so that  $\gamma_0 \ll 1/\nu$  in the present range of  $\gamma_0$ . This term could play a role when the

Coulomb interaction is so high that we are already in the Wigner crystal of solitons and no more comparison with the string phase is relevant. This yields  $\mu_{sol} \approx 2J_{\perp}/\sqrt{\nu}$ . The cohesion energy of the string is thus

$$E_c = J_{\perp} \left( \zeta + \frac{\gamma_D}{\sqrt{1 + \zeta^2}} \right) - \mu_{sol}. \quad (35)$$

From (35) we see clearly that in the absence of Coulomb interaction, which implies that  $\zeta = 0$ , the vertical string is stable. When the Coulomb interaction increases the tilt angle increases beyond the transition to the tilted phase. Thus  $E_c$  increases from negative values. As  $\zeta$ , being the optimal angle of the string, must satisfy (25), the maximum tilt angle  $\zeta_M$  corresponding to  $E_c = 0$  and the related coupling constant  $\gamma_{DM}$  read

$$\zeta_M = \frac{\mu_{sol}}{4J_{\perp}} + \frac{1}{2} \sqrt{\left( \frac{\mu_{sol}}{2J_{\perp}} \right)^2 - 2} \quad \gamma_{DM} = \frac{(1 + \zeta_M^2)^{3/2}}{\zeta_M}.$$

Thus, for a diluted system, with  $\mu_{kink} \approx 2J_{\perp}/\sqrt{\nu}$ , the maximum angle reads  $\zeta_M \approx 1/\sqrt{\nu} \gg \zeta_{opt1}^c$  and thus the melting of the string takes place above the transition to the tilted phase,  $\gamma_{DM} \gg \gamma_D^c$ , as it should be.

If we consider the full problem involving many domain lines, the latter form a 1D Wigner crystal with a lattice step equal to the screening length. Their inclination favors the transition to the triangular Wigner crystal of kinks. This transition can be detected as soon as Bragg peaks appear in the direction of the inclined strings.

## 6.2 The shape of the aggregates at non-zero temperature

More exotic is the non zero temperature case. We address here the question of the shape of the charged aggregates of solitons.

It has been shown in [8], with the help of a mapping to the ferromagnetic Ising model, that there are no strings, i.e. infinite domain lines of solitons, at non-zero temperature. The latter emerge from a process of exponential growth of aggregates of bisolitons below a crossover temperature  $T_{cr}$ . In the non-interacting case,  $T_{cr} = T_0$  and the aggregates are rods perpendicular to the chains of the quasi-one dimensional system, cf. Figure 9 a). At zero temperature the rods cross the whole system forming the free domain lines of solitons. In the interacting case the crossover temperature is lowered with respect to  $T_0$  and becomes Coulomb dependent. In the region between  $T_0$  and  $T_{cr}$  antiferromagnetic correlations take place in order for the bisolitons to aggregate, cf. [8]. This is due to the important size-charging energy of the aggregates. The latter must also determine the shape of the aggregates. We already know that, at zero temperature, strings tilt due to the Coulomb interaction. An inclined aggregate, as in Figure 9 c), would thus be more favorable than the straight rod. But at finite temperature angular kinks are present and they further reduce the Coulomb energy. It is shown in Appendix C that a droplet with the shape of Figure 9 b)

Figure 9: a) Rod in the absence of Coulomb interaction. The Coulomb energy of b) is lower than that of c). At finite temperature the aggregates thus have the b) shape.

Figure 10: Phase diagram of the 2D system as a function of the coupling constant  $\gamma_0$  and temperature  $T$ . Details are given in the text.

is favored in comparison with the previous aggregates. This is done by evaluating the energies of these aggregates  $\Delta E_b = E_b - E_b^{(se)}$  and  $\Delta E_c = E_c - E_c^{(se)}$  where their divergent self-energies  $E_b^{(se)}$  and  $E_c^{(se)}$  have been subtracted. For the aggregate c) the separation between the bikinks  $x_{opt}$  is taken as the equilibrium separation under the combined action of the Coulomb force  $(ze)^2/\epsilon x^2$  and the confinement one  $-J_\perp/a_x$ , i.e.  $x_{opt} = \sqrt{s\gamma_0}$ . Moreover, the tilt angle corresponds to the optimal one. In the confinement regime  $\gamma_0$  is related to  $\zeta$  with the help of (25). The regularized energies of the aggregates thus depend on one free parameter  $\zeta$ . The later must be larger than  $1/\sqrt{2}$  to be in the stable confinement regime. We find that the difference between these energies  $\Delta E_c - \Delta E_b > 0$  as a function of  $\zeta$  so that the energy of b) is always lower than that of c). This is strongly in favor of the existence of b)-like droplets at finite temperatures.

The results obtained in this section are summarized on the phase diagram Figure 10.

### 6.3 Application to uniaxial ferroelectrics

Recently a ferroelectric Mott-Hubbard state has been observed in quasi 1D organic superconducters such as  $(TMTCF)_2X$ . We give a brief account on the origin of this phase and connect the results to our present study. Experimental and theoretical results are given in detail in [2].

In the system mentioned above  $TMTCF$  are molecules composing the stacks and therefore giving rise to the one dimensional nature of the compound.  $X$  are ions placed in the vicinity of the molecules. At large temperatures, of the order of  $100K$ , the ions reorder through a uniform shift which gives rise to a ferroelectric phase. The latter has been detected via the measurement of the dielectric susceptibility which shows a gigantic anomaly at low frequency around  $T_{fe} \sim 150K$ . At low temperature domain lines, separating domains with opposite polarization, should be observed. Their existence is necessary to minimize the external electric field generated by charges accumulating at the boundary of the sample. Moreover, as the interface corresponds to a jump in the polarization it is charged. Following [2] we shall define as  $\alpha$ -solitons the elementary constituents of the interface which connect domains with opposite polarization. They carry a fractional charge  $ze$  with  $z = 2\alpha/\pi$ .

Two facts suggest that this system is a good candidate for the observation of

charged interfaces. First the background dielectric susceptibility  $\epsilon_0 \sim (\omega_p/\Delta)^2 \sim 10^4$  is large. Further more  $\pi$ -solitons are also present and they screen the Coulomb interaction. This weakens the Coulomb interaction. In such systems, the strings of  $\alpha$ -solitons should thus be stable against a melting towards a Wigner crystal. Aggregates of  $\alpha$ -solitons, as the ones described above, could also be observed at higher temperatures.

## 7 The 3D case

We consider briefly the important case of three dimensional systems where interfaces are domain walls. In 3D some rigorous statements allow a good understanding of the uncharged case in the frame of quasi-one dimensional systems, cf. [7]. In the presence of Coulomb interactions the problem becomes even more difficult. The study will therefore remain mainly qualitative. We will focus on the zero temperature properties of the charged 3D case. The main point is to check whether or not the solitonic lattice effectively orders in the form of domain walls. Noting that in the third direction,  $z$ , the coupling constant is  $J_z$  and the unit length  $a_z$  we will take  $J_z = J_y = J_{\perp}$  and follow [7] as well as our present experience of the charged 2D case.

### 7.1 Uncharged domain wall

For the non-interacting case it has been shown in [7] that peculiarities are brought by the raise of dimensionality. In 3D the excitations analogous to rods would be disc-like objects. However, rigorous statements concerning the 3D case show that, at a temperature  $T_3 \approx 8J_{\perp}/\ln(2/\nu) \ll T_c \approx J_{\perp}/\nu$ , a density  $\nu_c = \nu - \nu_n$  of solitons condense into infinite anti-phase domain walls perpendicular to the chains of the quasi-one dimensional system;  $\nu_n$  then corresponds to the density of finite size solitons below  $T_3$ . Therefore the crossover regime of growing rods, which took place below  $T_0$  in 2D, cannot take place in 3D. Instead a transition takes place at  $T_3$  which is a kind of real space Bose condensation. The effect of thermal fluctuations on the walls is well known. Several authors have shown ( see references in [12]) that, in 3D the hight-hight correlation function remains finite at  $T < T_R$  whereas it diverges logarithmically for  $T \geq T_R$ , where  $T_R > 0$  is the roughening temperature. From these considerations  $T_3$  may be considered as the roughening temperature. The existence of walls in 3D at finite temperatures is compatible with the fact that in Ising-like systems there is 2D long range order at low temperatures.

### 7.2 Charged domain wall versus Wigner crystal

The peculiarity of the domain wall, with respect to the domain line, is due to the large Coulomb energy of the former. The Coulomb potential decreases linearly with the distance  $\phi(x) = -|x|$ , where  $x$  is along the axis perpendicular to the untilted wall. This might considerably disfavor the existence of the charged wall

as can be shown with the help of the following estimations. We neglect thermal fluctuations for simplicity. We ask for the equilibrium position of a constituent soliton under the combined action of the Coulomb repulsion and the attractive elastic or confinement force. The Coulomb force  $(ze)^2/\epsilon s_\perp$ , where  $s_\perp = a_y a_z$  is the unit area of the wall, arises from the infinite wall and should be balanced by the short range force  $-J_\perp x^{p-1}/a_x^p$ , with  $p = 1, 2$  as before. The equilibrium position is thus  $x_{eq}^{p-1} = 2\gamma_0 a_x^p/a_z$  with  $\gamma_0$  given by (18).

In the elastic regime,  $p = 2$ , the equilibrium position of the soliton is given by  $x_{eq} = 2\gamma_0 a_x^2/a_z$ . This suggests that the charged straight wall still exists in the elastic regime. As in the case of the line, when  $\gamma_0$  increases the wall acquires a finite width  $x_{eq}$ , an indication that a shape instability takes place. We suggest that the wall is unstable towards an inclination and the ground state configuration is thus  $x(y, z) = \zeta z$ . This amounts to consider the wall as an ensemble of charged lines along the  $y$ -axis. We thus have a one-component, two-dimensional coulomb gas in the  $(x, z)$  plane which is confined along the  $z$ -axis. The related hamiltonian is

$$H = \frac{J_\perp}{s_\perp} \int dz (dx/dz)^2 - \frac{e^2}{\epsilon s_\perp^2} \int dz dz' \ln \left( \frac{\sqrt{(x(z) - x(z'))^2 + (z - z')^2}}{l_D} \right)$$

In the mean-field approximation, the free energy density is thus

$$f_{3D}^{(0)} \approx \frac{J_\perp}{s_\perp} [\zeta^2 - \gamma_{3D} \ln(1 + \zeta^2)] \quad (36)$$

where

$$\gamma_{3D} = \frac{(ze)^2}{\epsilon s_\perp J_\perp} l_D = \gamma_0 l_D / a_z$$

The transition to the tilted wall is here also second order as can be seen with the help of (36). The critical coupling constant is given by  $\gamma_0^c = 2/l_D \ll \gamma_0^{c(2D)} = 2/\ln l_D$ .

In the confinement regime, with  $p = 1$ , the raise of dimensionality has more crucial effects. In this case energy scales compete because both Coulomb and confinement energies are linear in  $x$ , the distance to the wall. As soon as the Coulomb energy scale is larger than the confinement energy scale the soliton cannot find its equilibrium position and the wall melts. Walls in the confinement regime could therefore be prohibited. However, a more favorable criterion can be obtained if we consider a tilted wall. If  $\zeta$  is sufficiently large, the component of the Coulomb force along the  $x$ -direction, which is reduced by  $1/\sqrt{1 + \zeta^2}$ , could be balanced by the confinement force. This defines the stability angle  $\zeta_s$  of the wall. Hence, in the confinement regime, the solitonic lattice might be observed either as a strongly tilted domain wall or as a liquid of solitons which might order in the form of a Wigner crystal.

Of course richer situations can be found due to the anisotropy of the system. In some systems, cf. the nickelate oxides below, a mixed confinement-elastic regime might take place. Namely, the wall could be in the confinement regime along the third direction and in the elastic regime in the planes or vice versa.

### 7.3 Application to oxides

In section 4.4 we have considered the case of  $La_{2-x}Sr_xCuO_4$ , i.e. *LSCO*, where diffuse magnetic peaks along the direction perpendicular to the  $CuO_2$  planes, i.e. the  $z$ -direction, where the signature of string-like stripes. Other experimental results concerning  $La_{1.6-x}Nd_{0.4}Sr_xCuO_4$  and the nickelate  $La_{2-x}Sr_xNiO_{4+\delta}$  show a  $3D$  ordering of charge stripes, cf. [3] and references therein. The impact of the pinning by the lattice and the Coulomb interactions where shown to play a crucial role in these systems.

In  $La_{1.6-x}Nd_{0.4}Sr_xCuO_4$  neutron diffraction studies have revealed diffuse magnetic peaks along the  $z$ -direction, in the stripe phase, as in *LSCO*. However, X-ray studies reveal that stripes are parallel in next-nearest-neighboring layers. Between layers the stripes are orthogonal. This  $3D$  ordering is due to a pinning of the stripes by the lattice structure.

The case of nickelates is more interesting. In  $La_{2-x}Sr_xNiO_{4+\delta}$  there is a body-centered stacking of parallel stripes with only weak perturbations due to the lattice. This  $3D$  ordering is due to Coulomb repulsion and corresponds, in relation with the previous subsection, to the presence of tilted domain walls. The step-like ordering from layer to layer suggests that confinement is present along the  $z$ -axis. On the other hand stripes in the  $NiO_2$  planes might be rigid which favors an elastic regime in the layers; no evidence for a shape instability has however been detected to our knowledge.

## 8 Conclusion

The statistics of charged interfaces, strings and walls, has been studied. We have found that shape instabilities, due to competing interactions, play a fundamental role. They manifest themselves through zero-temperature phase transitions from which new ground-states emerge where the interface is tilted. The  $2D$  case of the string has been extensively studied. For small tilt angles the string is elastic and the transition to the tilted ground state is second order. On the other hand a first order transition takes place if we are beyond the limit of validity of the elastic regime, i.e. in the confinement regime. At non-zero temperatures it has been shown that in either regimes roughening of the string, through the proliferation of angular-bikinks, destroys the long range positional order as soon as  $T > 0$ . At higher temperatures angular-kinks are thermally activated and destroy the long-range orientational order. These results have been confirmed with the help of a numerical approach based on the Montecarlo-Metropolis algorithm. We have then related the present study to the general problem of the statistics of solitons in charge-density wave systems. In such systems the string has been shown to emerge from bubble-like aggregates of solitons upon decreasing temperature. When the Coulomb interaction is large the string melts towards a Wigner crystal of solitons. Applications concerning charged strings in uniaxial ferroelectric experiments have also been considered. Finally we have treated mostly qualitatively the more realistic  $3D$  case of a charged wall. The

latter, when charged, is also submitted to instabilities towards a tilted phase in the elastic regime. In the confinement regime, the solitons might order in the form of a wall with a definite tilt angle as in nickelate oxides or as a liquid.

## Acknowledgments

I would like to thank S Brazovskii for crucial, both helpful and inspiring, discussions from the very beginning of this work. I would like to thank A. R. Bishop for his hospitality at the Theoretical Division, Center of Non-Linear Studies, of Los Alamos where part of the numerical work has been done. I am also grateful to F. Cornu and B. Jancovici for useful remarks concerning screening in Coulomb fluids.

## Appendix A

In this appendix we give some details on the screening in the ensemble of solitons. Screening makes the energy extensive and gives a meaning to the thermodynamic limit as has been said all along the paper. In the following we will work in the RPA approximation which is very well known in the field on many-body theory. This allows us to derive the Debye length and the electrostatic potential in two cases: two and three-dimensional screening.

We consider first a single plane embedded in  $3D$  space. This case corresponds to two-dimensional screening. Supposing the Coulomb field  $\phi$  slowly varying, it obeys the following semi-classical equation

$$-\epsilon\Delta\phi(\vec{R}) = -4\pi e^2(\Pi^{(0)} * \phi)(\vec{R})\delta(z) + 4\pi e^2\rho_0(\vec{r})\delta(z) \quad (37)$$

where  $\vec{R}$  is a  $3D$  vector associated with the  $3D$  Coulomb field,  $\vec{r}$  is a  $2D$  vector indexing the charges which are embedded in the  $z = 0$  plane and  $\rho_0$  is some external charge.  $\Pi^{(0)}(x, y)$  is the response function, or polarization part, of the soliton system which is related to the correlation function by fluctuation dissipation theorem

$$T\Pi^{(0)}(\vec{r}) = <\delta\rho(\vec{r})\delta\rho(\vec{0})> \quad (38)$$

where  $\delta\rho(\vec{r}) = \rho(\vec{r}) - \nu$ ,  $\rho(\vec{r})$  being the density of solitons and  $\nu$  the background neutralizing charge.

The first term on the right of (37) corresponds to the screening charge. This term implies linear screening and dispersion via the convolution. The Coulomb field is then

$$\phi(\vec{k}, z = 0) = \frac{2\pi e^2\rho_0(\vec{k})}{\epsilon|k| + 2\pi e^2\Pi^{(0)}(\vec{k}, z = 0)} \quad (39)$$

where  $\vec{k}$  is the reciprocal vector associated with  $\vec{r}$ . The fact that the potential is evaluated at  $z = 0$  implies that the field lines are confined to the same space

as the particles, cf. [13]. Expression (39) leads to the Debye screening of the field with a Debye length

$$\frac{1}{l_{2D}} = \frac{2\pi e^2}{\epsilon} \Pi^{(0)}(k = 0). \quad (40)$$

Also the  $k$ -term in the denominator of (39) is a feature of  $2D$ -systems. In real space this leads to an algebraic screening instead of the exponential one, cf. [13] for detailed studies of screening effects in Coulomb fluids and below for an example.

We consider now the three dimensional case of independent planes embedded in a neutral media. Such a system of decoupled planes brings a  $3D$ -screening. The screening charge is then a function of the three-dimensional vector  $\vec{R}$ . But, as the planes are independent, the bare correlation function corresponds to  $\Pi^{(0)}(\vec{R}) = \Pi^{(0)}(\vec{r})\delta(z)$ . By the same arguments as in the first section we can compute the coulomb field which reads

$$\phi_{3D}(\vec{K}) = \frac{4\pi e^2 \rho_0(\vec{K})}{\epsilon K^2 + 4\pi e^2 \Pi^{(0)}(\vec{k}, z = 0)/a_z} \quad (41)$$

where we consider only the  $z = 0$  plane subject to the bulk screening. The three-dimensional Debye length is then given by

$$\frac{1}{l_{3D}^2} = \frac{4\pi e^2}{\epsilon a_z} \Pi^{(0)}(k = 0) \quad (42)$$

where  $a_z$  is the inter-plane distance. In real space (41) leads to the usual exponential screening.

Finally we derive the polarization part for the present problem. This gives explicit expressions for the screening lengths and for  $\phi(\vec{r})$ . Below the crossover transition  $T_0$

$$T\Pi^{(0)}(x, y) \approx \frac{1}{2s^2} \nu a_x \exp\left(-\frac{2y}{l_\perp}\right) (2\delta(x) + \delta(x + a_x) + \delta(x - a_x)) \quad (43)$$

corresponding to the aggregation of the solitons into rods of length  $l_\perp$ , cf. [7]. Fourier transforming (43) we get

$$T\Pi^{(0)}(\vec{k}) \approx \frac{\nu}{4sa_y} (1 + \cos(k_x a_x)) \frac{l_\perp}{1 + k_y^2 l_\perp^2 / 4}.$$

Thus  $\Pi^{(0)}(\vec{k}) \approx \frac{\nu l_\perp}{2sa_y T}$  and, as we work at constant density of solitons  $\nu$ ,  $l_\perp \approx \sqrt{2\nu} \exp(2J_\perp/T)$ . With the help of (40) and (42), this yields

$$l_{2D} = \frac{2\epsilon sa_y T}{\pi e^2 (2\nu)^{3/2}} \exp\left(-\frac{2J_\perp}{T}\right) \quad l_{3D} = \sqrt{\frac{\epsilon sa_z T}{\pi e^2 (2\nu)^{3/2}}} \exp\left(-\frac{J_\perp}{T}\right). \quad (44)$$

In the  $2D$ -screening regime, the field can then be written, in the long distance limit with respect to the coarse graining length  $a_x$

$$\phi(\vec{k}) = \frac{2\pi e^2}{\epsilon} \frac{1 + k_y^2 l_\perp^2 / 4}{|k|(1 + k_y^2 l_\perp^2 / 4) + 1/l_D} \quad (45)$$

which reflects the anisotropy of the problem. To give an idea of the algebraic screening we Fourier transform (45) in the limit  $k_y l_\perp \rightarrow 0$ , i.e. far enough from the rod. This yields

$$\phi(\vec{r}) \approx \frac{2\pi e^2}{\epsilon} \frac{(2l_D)^2}{r^3} + O\left(\left(\frac{l_D}{r}\right)^4\right)$$

in the limit  $r \gg l_D$ . We see that the algebraic tail leads to a slow decay of the potential in contrast to the usual exponential one. However this dipolar-type of interaction, beyond the screening length, is compatible with the growth of the aggregates, cf. [8].

## Appendix B

Our purpose is mainly to show the differences and common points between the two interface models. The approach is based on the transfer matrix technic. In the present case, this formulation cannot be used straight forwardly because of the long-range interactions in (10). Some results obtained in the non-interacting case should however remain in the presence of the long range interaction. It is on such a property that we focus now.

The associated Hamiltonian of the problem is

$$\beta H_p = \frac{K}{a^{p-1}} \sum_{y=0}^{L-1} |x_{y+1} - x_y|^p \quad (46)$$

where the short distance cut off has been taken explicitly into account. The transfer matrix  $\widehat{T}_a$  is defined as an integral operator with eigenfunctions  $\psi(x)$  whose kernel is expressed in terms of (46). Namely

$$\widehat{T}_a \psi(x) = \int dx' \exp\left(-\frac{K}{a^{p-1}} |x - x'|^p\right) \psi(x'). \quad (47)$$

The free problem is simple enough to be treated just with the integral equation (47). For a more exhaustive account on the general results one can obtain with help of the transfer matrix technic see [14], who is dealing with the problem of an elastic string in an external potential.

For both models the eigenfunctions of the transfer matrix are simply plane waves

$$\psi_k(x) \approx \exp(ikx).$$

This amounts to Fourier transform the kernel of (47). The eigenvalues of the transfer matrix associated to both interface models are thus

$$\epsilon_k^G \approx \frac{k^2}{2K} \quad \epsilon_k^{SOS} \approx \log(K^2 + k^2). \quad (48)$$

By comparing the two spectrums in (48) we see clearly that both models have the same long distance, i.e.  $k \rightarrow 0$ , properties.

## Appendix C

In this appendix we give some details relative to the evaluation of the energies of the aggregates b) and c) of Figure 9. The calculations are analogous to the ones for the angular kinks.

The energy of aggregate b is given by:

$$\Delta E_b = 2E_{b1} + 2E_{b2} + 2E_{b3} \quad (49)$$

with, for example,  $E_{b1}$  being given by the first term in (29) for the angular kink energy. That is

$$E_{b1} = \frac{J_{\perp}\gamma_0}{a_y} \int_{-L}^{t_1} dt \int_{t_1}^L dt' \frac{1}{\sqrt{(t-t')^2 + (x_1(t) - x_2(t'))^2}}$$

where  $t_1$  denotes the position of the kink along the  $y$  axis,  $2L$  is the total length of the aggregate along the same axis and  $x_{1,2}(t) = \pm\zeta(t - t_1) - x_1$ .

The same kind of expressions can be obtained for the other terms in (49) which correspond to interactions between other parts of the aggregate: adjacent parts for  $E_{b1}$  and  $E_{b2}$  and opposite, parallel, parts for  $E_{b3}$ . This yields

$$\begin{aligned} E_{b1} &= \frac{J_{\perp}\gamma_0 L}{a_y \sqrt{1 + \zeta^2}} \log \left( 1 + \sqrt{1 + \zeta^2} \right) \\ E_{b2} &= \frac{J_{\perp}\gamma_0 L}{a_y \sqrt{1 + \zeta^2}} \log \left( \frac{\zeta + \sqrt{1 + \zeta^2}}{\zeta} \right) \\ E_{b3} &= \frac{J_{\perp}\gamma_0 L}{a_y \sqrt{1 + \zeta^2}} \left( 1 - \frac{1 + |\zeta|}{\sqrt{1 + \zeta^2}} \right) + \\ &+ \frac{J_{\perp}\gamma_0 L}{a_y (1 + \zeta^2)^{3/2}} \left( \log \left( 1 + \sqrt{1 + \zeta^2} \right) + 2\zeta^2 \log \left( \frac{|\zeta| + \sqrt{1 + \zeta^2}}{|\zeta|} \right) \right) \end{aligned}$$

For the second aggregate we have

$$\Delta E_c = 2E_{c1} + 2E_{c2} + E_{c3} + E_{c4}$$

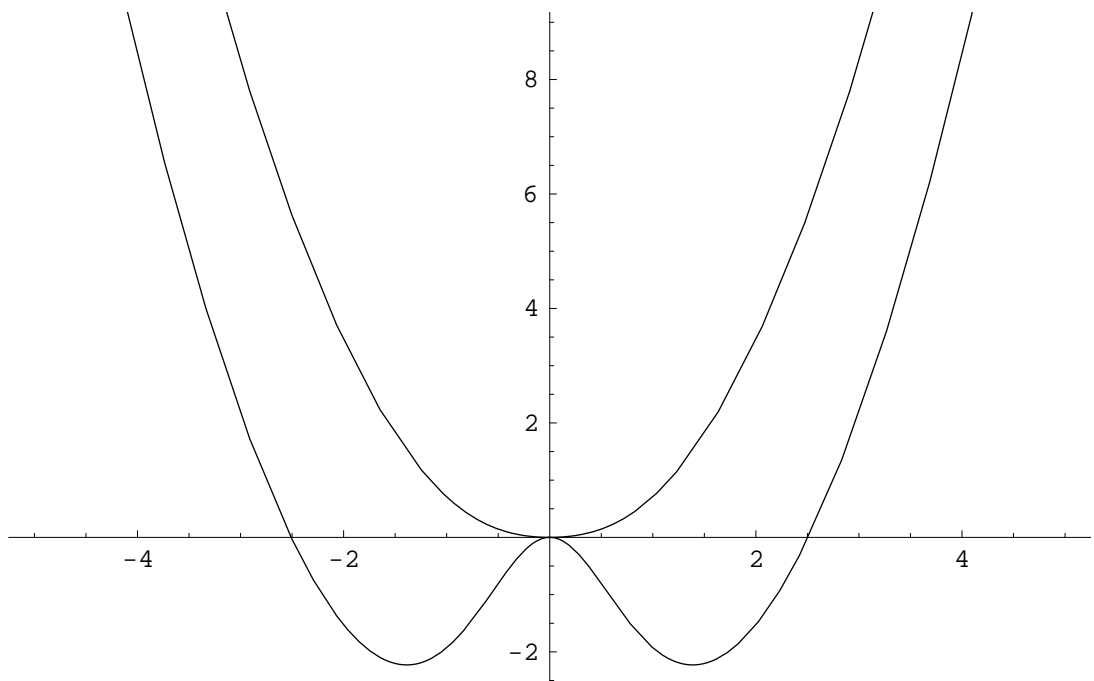
where  $E_{c1}$  and  $E_{c2}$  correspond to interactions of adjacent parts of the aggregate, while the two others correspond to interaction of opposite, parallel parts. The same kind of calculations as above lead to

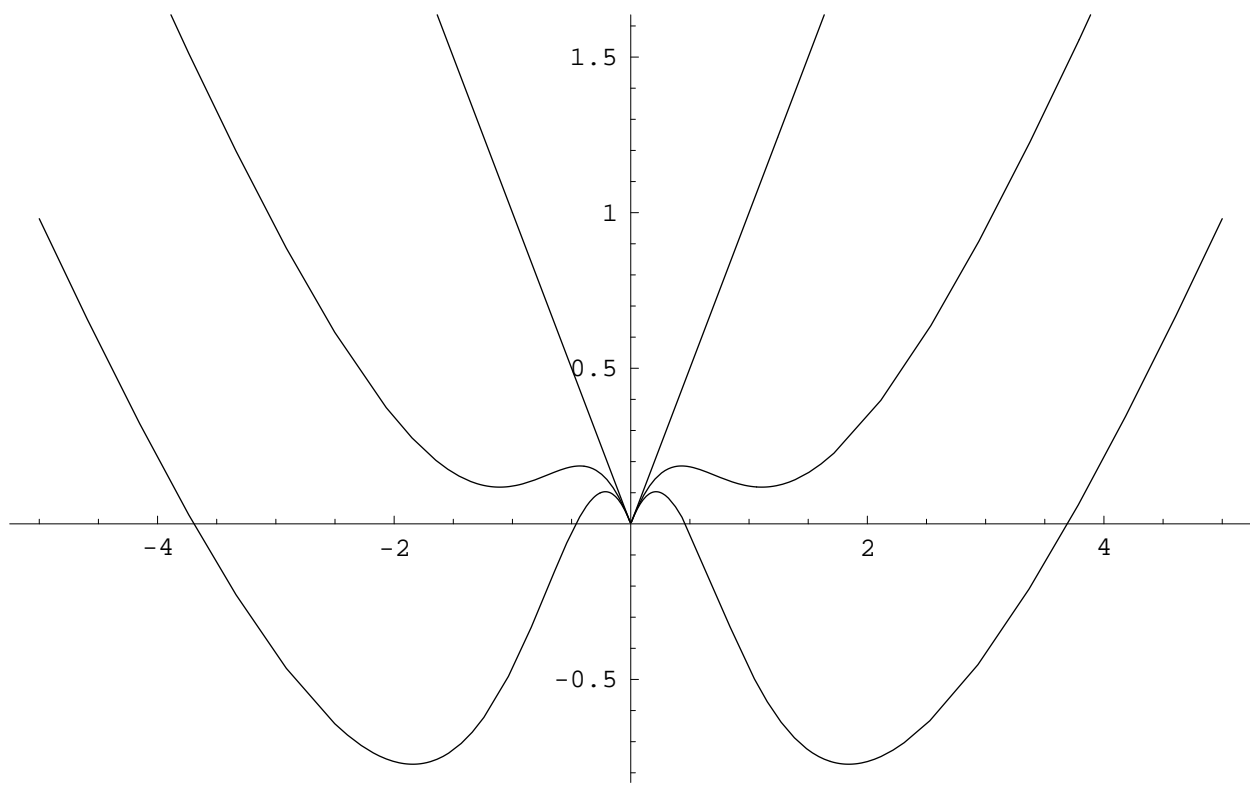
$$\begin{aligned}
E_{c1} &= \frac{J_{\perp} \gamma_0 L}{a_x} \log \left( \frac{2L\zeta + x_{opt} + \sqrt{4L^2 + (2L\zeta + x_{opt})^2}}{2L \left[ \zeta + \sqrt{1 + \zeta^2} \right]} \right) + \\
&+ \frac{J_{\perp} \gamma_0 L}{a_x \sqrt{1 + \zeta^2}} \log \left( \frac{2L(1 + \zeta^2) + \zeta x_{opt} + \sqrt{(1 + \zeta^2)(4L^2 + (2L\zeta + x_{opt})^2)}}{x_{opt} \left( \zeta + \sqrt{1 + \zeta^2} \right)} \right) \\
E_{c2} &= \frac{J_{\perp} \gamma_0}{a_x \sqrt{1 + \zeta^2}} \left\{ L \log \left( \frac{x_{opt} + \sqrt{x_{opt}^2 + 4L^2}}{2L} \right) \right. \\
&+ L\zeta \log \left( \frac{(x_{opt} + 2L\zeta) \left( 1 - 1/\sqrt{1 + \zeta^2} \right)}{\sqrt{x_{opt}^2 + 4L^2} + (x_{opt}\zeta - 2L)/\sqrt{1 + \zeta^2}} \right) + \\
&\left. + \frac{x_{opt}}{2} \log \left( \frac{(x_{opt} + 2L\zeta) \left( 1 + \zeta/\sqrt{1 + \zeta^2} \right)}{\sqrt{x_{opt}^2 + 4L^2} + (x_{opt}\zeta - 2L)/\sqrt{1 + \zeta^2}} \right) \right\} \\
E_{c3} &= \frac{J_{\perp} \gamma_0}{a_x} \left\{ \frac{1}{\sqrt{1 + \zeta^2}} \left[ 2x_{opt} - \sqrt{4L^2 + (x_{opt} - 2L\zeta)^2} - \sqrt{4L^2 + (x_{opt} + 2L\zeta)^2} \right] - \right. \\
&- 2L \log \left( \frac{x_{opt}\zeta - 2(1 + \zeta^2)L + \sqrt{(1 + \zeta^2)(4L^2 + (x_{opt} - 2L\zeta)^2)}}{x_{opt}^2} \right) - \\
&- 2L \log \left( \frac{-x_{opt}\zeta - 2(1 + \zeta^2)L + \sqrt{(1 + \zeta^2)(4L^2 + (x_{opt} + 2L\zeta)^2)}}{x_{opt}^2} \right) - \\
&- \frac{x_{opt}\zeta}{1 + \zeta^2} \log \left( -x_{opt}\zeta + 2(1 + \zeta^2)L + \sqrt{(1 + \zeta^2)(4L^2 + (x_{opt} - 2L\zeta)^2)} \right) - \\
&- \frac{x_{opt}\zeta}{1 + \zeta^2} \log \left( -x_{opt}\zeta - 2(1 + \zeta^2)L + \sqrt{(1 + \zeta^2)(4L^2 + (x_{opt} + 2L\zeta)^2)} \right) + \\
&\left. + \frac{2x_{opt}\zeta}{1 + \zeta^2} \log \left( x_{opt} \left( \zeta + \sqrt{1 + \zeta^2} \right) \right) \right\} \\
E_{c4} &= \frac{J_{\perp} \gamma_0}{a_x} \left\{ 4L \sqrt{1 + \zeta^2} - \sqrt{4L^2 + (x_{opt} - 2L\zeta)^2} - \sqrt{4L^2 + (x_{opt} + 2L\zeta)^2} + \right. \\
&\left. + x_{opt} \log \left( \frac{2L\zeta + x_{opt} + \sqrt{4L^2 + (2L\zeta + x_{opt})^2}}{2L\zeta - x_{opt} + \sqrt{4L^2 + (2L\zeta - x_{opt})^2}} \right) \right\}
\end{aligned}$$

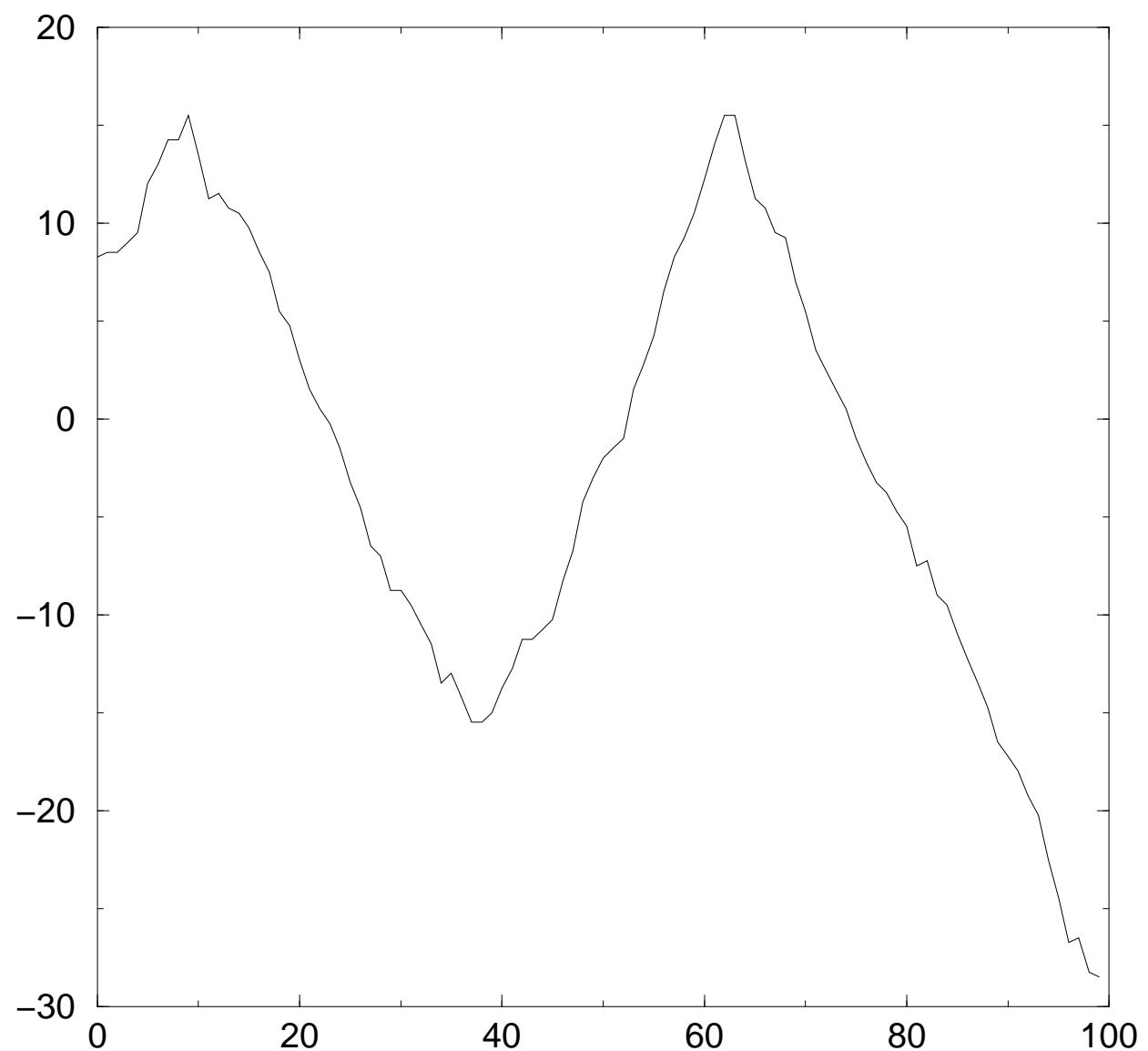
$$2L\zeta \log \left( \frac{\left( 2L\zeta + x_{opt} + \sqrt{4L^2 + (2L\zeta + x_{opt})^2} \right) \left( 2L\zeta - x_{opt} + \sqrt{4L^2 + (2L\zeta - x_{opt})^2} \right)}{4L^2 (\zeta + \sqrt{1 + \zeta^2})} \right)$$

## References

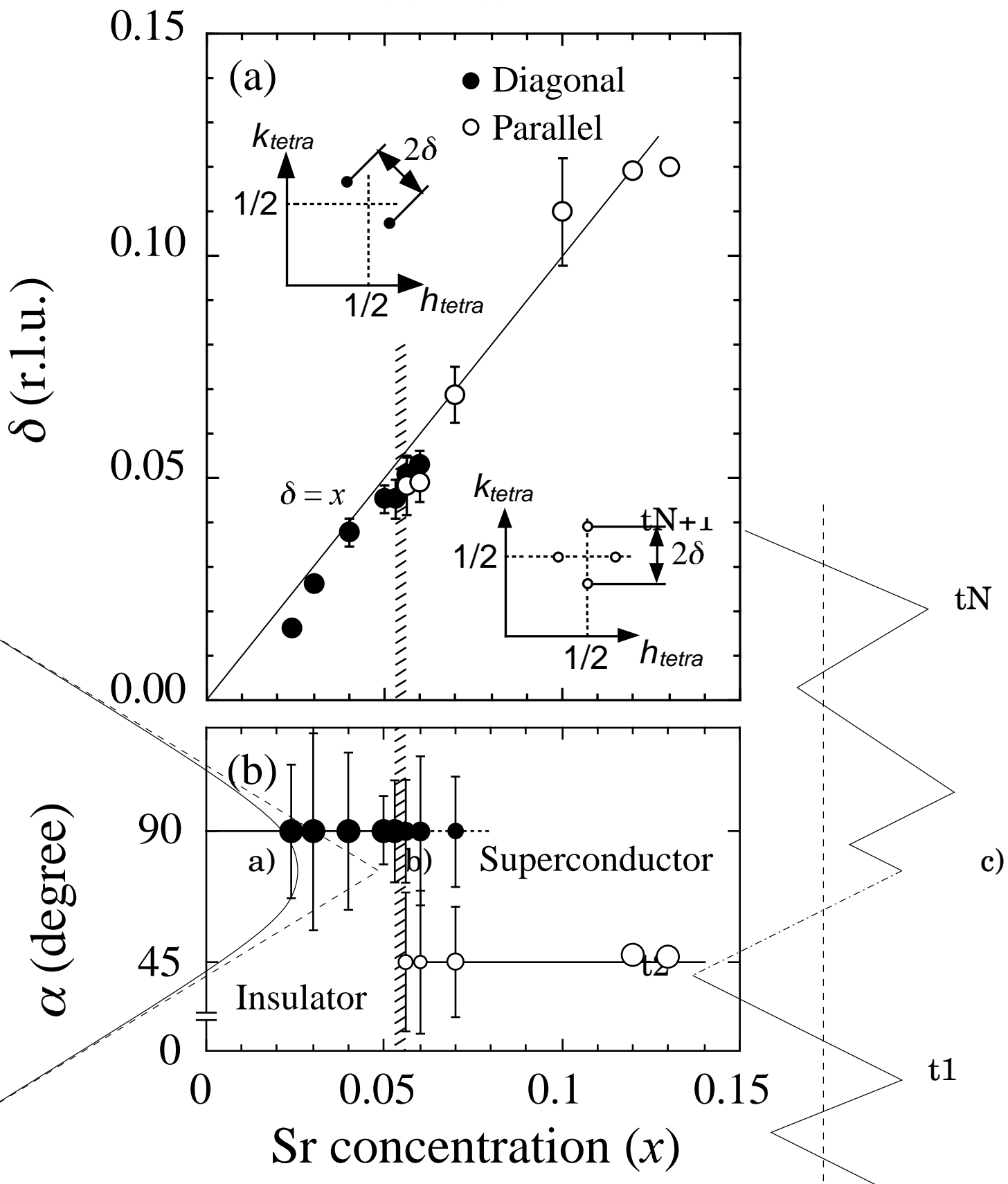
- [1] Schon J H, Berg S, Kloc Ch and Battlogg B 2000, *Science*, **287**, 1022
- [2] P Monceau, F Ya Nad and S Brazovskii, 2001, cond-mat/0012237
- [3] Tranquada J M, 1998, *Neutron Scattering in Layered Copper Oxide Superconductors*, ed A Furrer (Dordrecht: Kluwer)
- [4] M Bosch, W van Saarloos and J Zaanen, cond-mat/0003236
- [5] S Wakimoto & al, cond-mat/9908115; M Fujita, K Yamada & al. cond-mat/0101320
- [6] P Dai & al. *Phys. Rev. Lett.* **85** (2000) 2553
- [7] T Bohr and S Brazovskii, 1983, *J. Phys. C: Solid State Phys* **16** 1189
- [8] S Teber, B P Stojkovic, S A Brazovskii and A R Bishop, *J. Phys.: Condens. Matter* **13** (2001) 4015-4031
- [9] P A Lee, T M Rice and P W Anderson, *Solid State Comm.* **14** (1974) 703
- [10] S Brazovskii and N Kirova 1984 *Physics (Soviet Scientific Reviews Section A)* vol 5, ed I M Khalatnikov (New York: Harwood Academic) p 99
- [11] M J Rice, A R Bishop, J A Krumhansl and S E Trullinger 1976 *Phys. Rev. Lett.* **36** 432
- [12] G Forgacs & al *Phase Transitions and Critical Phenomena* vol 14, ed C Domb and J L Lebowitz (London: Academic)
- [13] F Cornu, *These d'habilitation* (1998); F Cornu, 1996, *Phys. Rev. E.*, **53**, 4595; B Jancovici, 1995, *J. of Stat. Phys.*, **80**, 445
- [14] R A Suris *Soviet. Phys. JETP* **20** (1965) 961



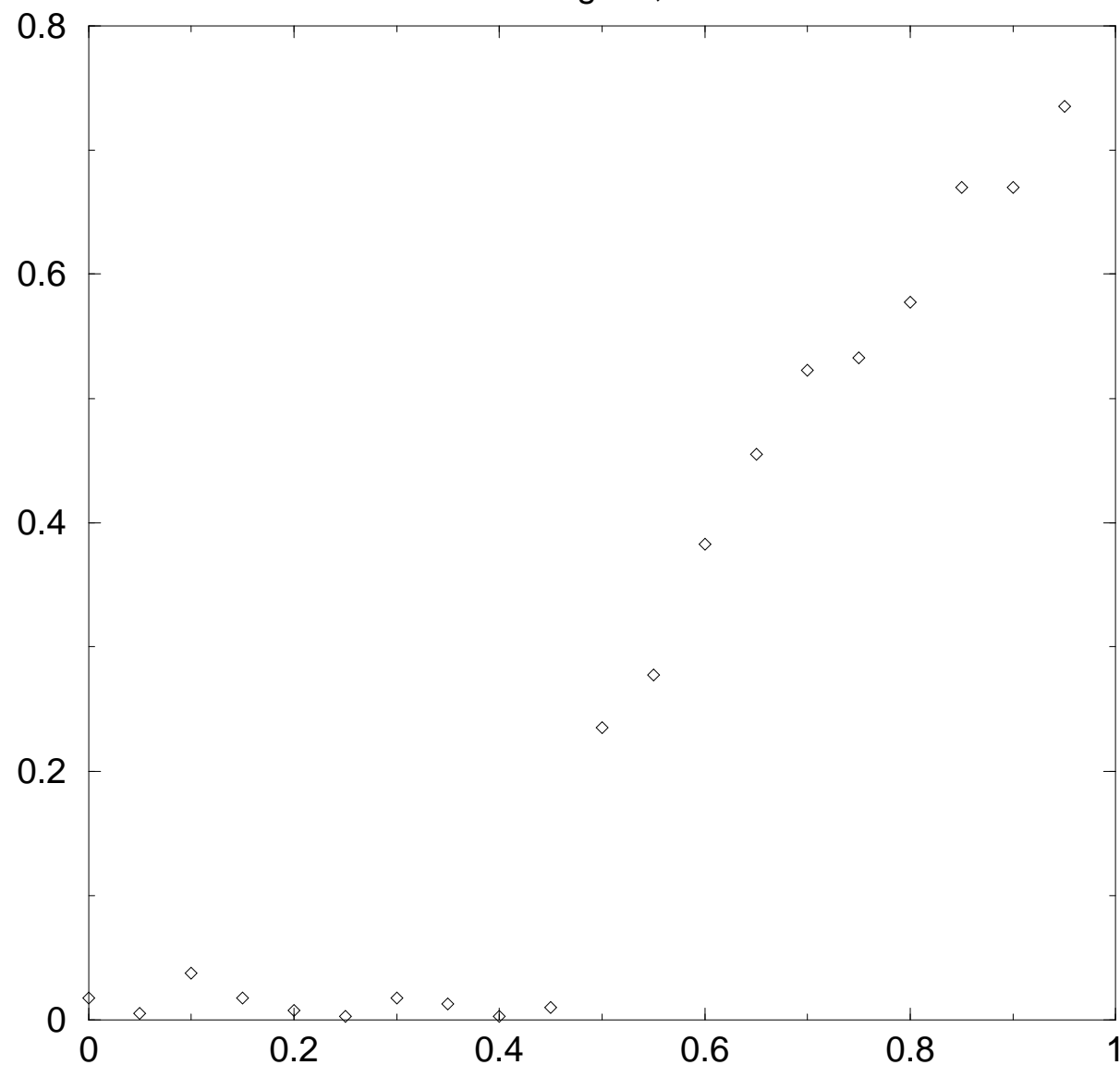


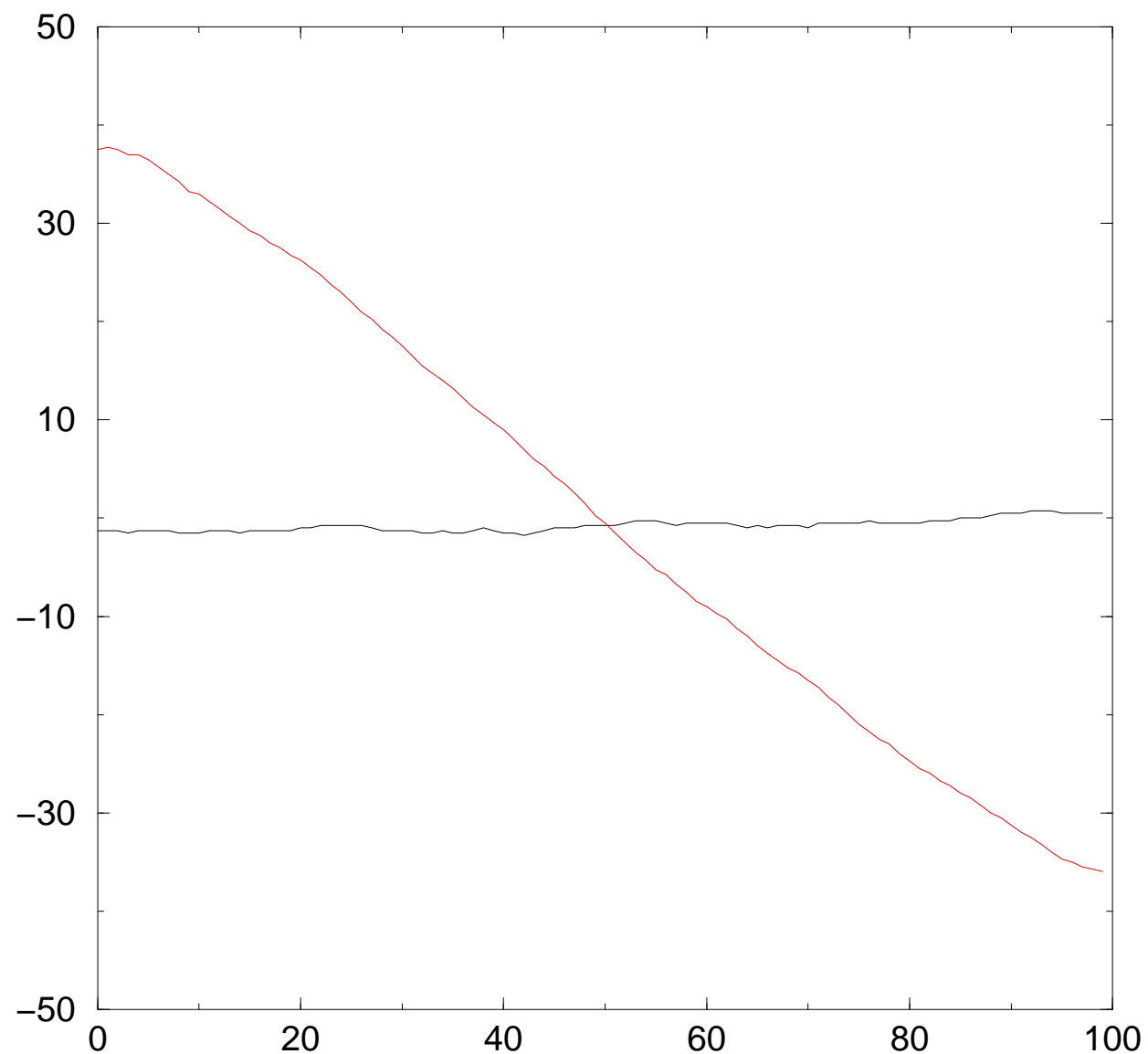


# $\text{La}_{2-x}\text{Sr}_x\text{CuO}_4$

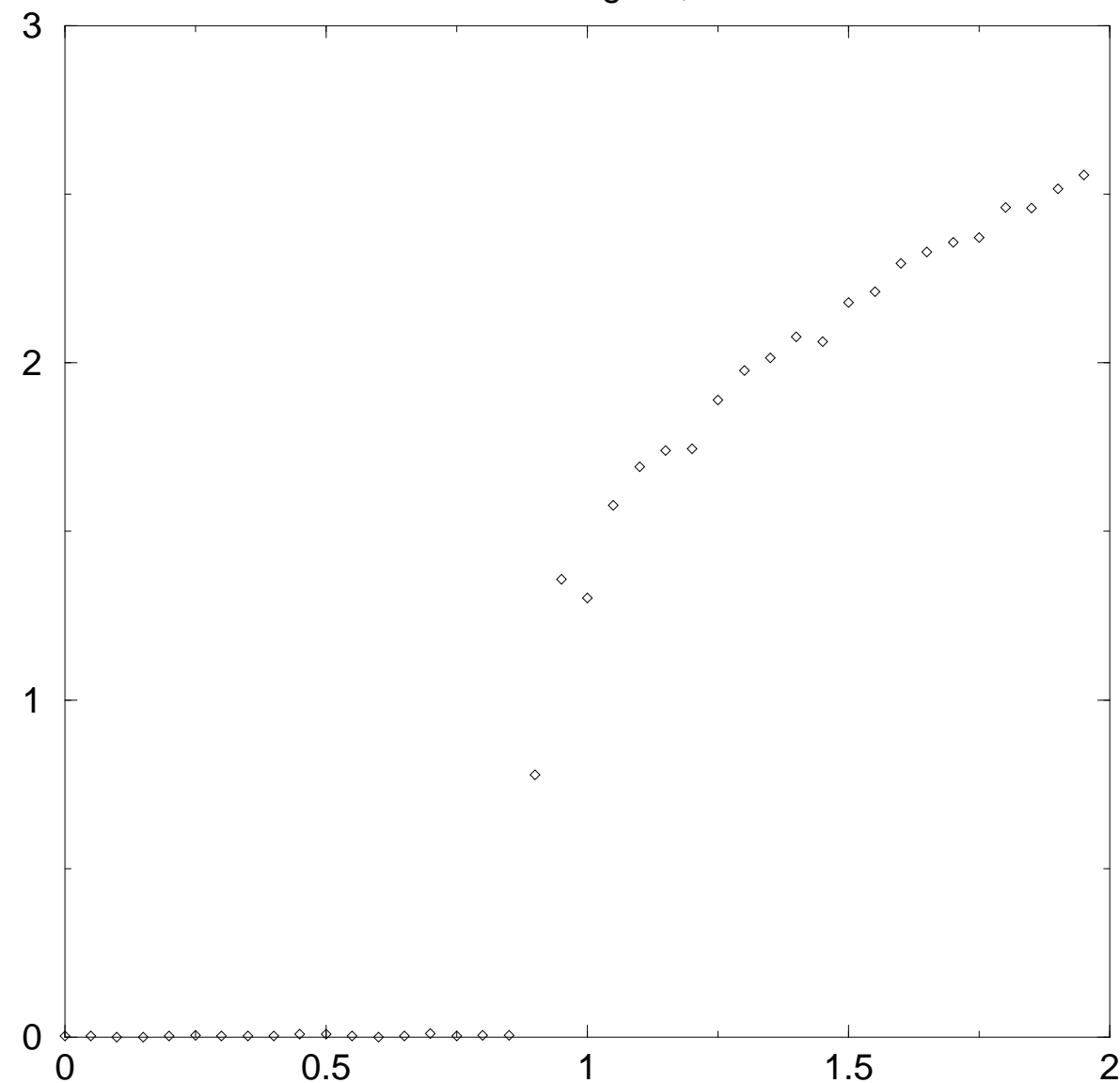


Elastic regime,  $L=100$





confinement regime,  $L=100$



confinement regime,  $L=100$

